Self-consistent phonon inputs for vibrationally corrected combinatorial nuclear level densities*

Jing-Zhu Hao (郝径竹) Nuo-Cheng Tang (唐诺程) Guan-Bin He (何冠彬) Yuan Tian (田源)†
Ying Cui (崔莹) Rui-Rui Xu (续瑞瑞)‡

China Nuclear Data Center, China Institute of Atomic Energy, Beijing 102413, China

Abstract: Phenomenological vibrational prescriptions are widely used in microscopic combinatorial nuclear level-density (NLD) calculations, but they introduce empirical phonon-energy systematics that are not generated by the underlying nuclear-structure model. This empirical input limits the predictive consistency of the model, especially for nuclei for which low-lying collective spectra are unavailable. To reduce this empirical component, we construct self-consistent phonon inputs for vibrationally corrected combinatorial NLDs by calculating the first 2^+, 3^-, and 4^+ phonon states with the relativistic quasiparticle random-phase approximation (RQRPA) built on the relativistic Hartree–Bogoliubov ground state. The corresponding RQRPA excitation energies are used in place of the phenomenological phonon energies, while the intrinsic combinatorial density and the established combinatorial vibrational prescription are kept unchanged. The method is benchmarked in selected even-even Sn isotopes against the phenomenological prescription and Oslo-normalized level densities. The RQRPA-based calculation approximately preserves the average vibrational enhancement of the phenomenological prescription and achieves agreement with the Oslo-normalized data comparable to that of the phenomenological calculation. These results demonstrate, for the selected semi-magic Sn isotopes, that self-consistent microscopic phonon energies can serve as collective inputs for vibrationally corrected combinatorial NLDs without using experimental low-lying spectra as model inputs.

Keywords: nuclear level density, self-consistent phonon inputs, relativistic quasiparticle random-phase approximation, combinatorial model, vibrational correction

DOI: 10.1088/1674-1137/aea283 **CSTR:** 32044.14.ChinesePhysicsC.50114112

I. INTRODUCTION

Nuclear level densities (NLDs) describe the number of available nuclear states at a given excitation energy, spin, and parity. They are indispensable inputs to Hauser–Feshbach reaction calculations and therefore enter evaluated nuclear data, activation analyses, reactor applications, and astrophysical reaction-rate calculations. Since Bethe's Fermi-gas description [1, 2], NLD models have evolved from global analytical prescriptions to microscopic approaches that incorporate shell structure, pairing correlations, deformation, and spin–parity distributions [3−17]. Among these, microscopic combinatorial methods provide a predictive framework by constructing many-quasiparticle configurations from single-particle spectra [10, 17−22]. Recent developments in microscopic NLD calculations have focused on improving the treatment of collective correlations, pairing effects, and predictive descriptions beyond experimentally known regions. Covariant density functional approaches, including relativistic Hartree–Bogoliubov frameworks, provide self-consistent descriptions of shell evolution and quasiparticle properties, while QRPA-based approaches enable microscopic descriptions of low-lying collective excitations [21, 23−27]. These advances provide a natural framework for reducing empirical ingredients in nuclear-data-oriented NLD calculations. More specifically, microscopic studies have emphasized the importance of a consistent treatment of collective correlations when extending NLD predictions to regions where experimental spectroscopic information is incomplete. In the present work, the intrinsic basis is generated with relativistic Hartree–Bogoliubov (RHB) theory, which describes the mean field, spin–orbit interaction, pairing correlations,

Received 15 July 2026; Accepted 2 September 2026; Accepted manuscript online 3 September 2026

* This work was supported by the National Key Research and Development (R&D) Program (2022YFA1602403), the "Ye Qisun" Science Foundation of the National Natural Science Foundation of China (U2541242), the Key Program of the National Natural Science Foundation of China (KZ77088701), the National Natural Science Foundation of China (U2441221), and the IAEA Research Contract (28681)

† E-mail: tiany@ciae.ac.cn

‡ E-mail: xuruirui@ciae.ac.cn

©2026 Chinese Physical Society and the Institute of High Energy Physics of the Chinese Academy of Sciences and the Institute of Modern Physics of the Chinese Academy of Sciences and IOP Publishing Ltd. All rights, including for text and data mining, AI training, and similar technologies, are reserved.

and shell evolution within a common energy-density functional [23−26]. A remaining issue in such microscopic NLD calculations is how collective enhancement is introduced.

Experimentally, NLDs are constrained by known discrete-level schemes at low excitation energy, neutron-resonance information near the separation energy, and Oslo-type measurements in the quasicontinuum region [28, 29]. These developments provide increasingly stringent benchmarks for microscopic NLD models and motivate predictive calculations for nuclei where complete spectroscopic information is unavailable.

The intrinsic combinatorial density constructed from quasiparticle configurations does not, by itself, fully account for the additional states associated with low-lying collective motion. In many nuclear-data-oriented NLD models, vibrational effects are therefore included through phenomenological enhancement factors or empirical phonon energies. These prescriptions are practical and successful in reproducing average systematics, but the collective input is then partly disconnected from the microscopic model that generates the intrinsic density. This hybrid character limits the predictive consistency of the calculation, especially for nuclei where measured low-lying collective spectra are unavailable.

A natural way to reduce this empirical component is to generate the vibrational phonon energies from the same microscopic framework that provides the intrinsic quasiparticle basis. The relativistic quasiparticle random-phase approximation (RQRPA) is well suited for this purpose because it describes small-amplitude collective excitations on top of the RHB ground state. RQRPA phonon energies can therefore serve as self-consistent microscopic inputs for the vibrational correction of combinatorial NLDs. The key question is whether such microscopic phonon inputs can approximately preserve the successful average effect of the empirical vibrational prescription.

Here we address this question for selected even-even Sn isotopes. The semi-magic Sn chain is close to spherical and provides a clean benchmark for low-lying 2^+, 3^-, and effective 4^+ collective inputs. The intrinsic RHB-based combinatorial density and the combinatorial vibrational prescription are kept fixed, while the empirical phonon energies are replaced by RQRPA-calculated values. This controlled setup isolates the effect of changing the collective phonon input without modifying the intrinsic density or the established combinatorial vibrational prescription.

The purpose of the present work is not to tune RQRPA phonons to known Sn NLDs, but to test whether empirical vibrational inputs can be replaced by self-consistent microscopic phonon energies while approximately preserving the average phenomenological enhancement. Section II summarizes the RHB, RQRPA, and combinatorial framework. Section III presents the controlled benchmark, including phonon-energy comparisons, systematic NLD results, and channel diagnostics near S_n. Section IV gives the conclusions and outlook.

II. THEORETICAL FRAMEWORK

The calculation is designed as a controlled replacement test. The intrinsic RHB-based combinatorial density and the combinatorial vibrational prescription are kept fixed; only the phonon energies are changed from empirical systematics to RQRPA values. The term self-consistent phonon input refers here to the microscopic determination of the phonon excitation energies; the combinatorial vibrational prescription itself remains identical to that used in the phenomenological reference calculation. Thus, the RHB spectrum provides the intrinsic basis, while the RQRPA phonons provide the microscopic collective input used in the same NLD calculation.

A. Microscopic Inputs from RHB and RQRPA

The ground-state quasiparticle basis is generated by self-consistent spherical RHB calculations with the nonlinear meson-exchange interaction NL3 [30−32] in the particle–hole channel and the finite-range separable pairing force of Refs. [33, 34] in the particle–particle channel. The pairing strength and range are taken as $G = 728$ MeV fm^3 and $a = 0.644$ fm, respectively. The resulting quasiparticle wave functions define the canonical basis used in the RQRPA calculation.

The calculations are performed for the selected even-even isotopes ^{112}Sn, ^{116}Sn, ^{118}Sn, ^{120}Sn, ^{122}Sn, and ^{124}Sn. The RHB calculations were performed in a spherical harmonic-oscillator basis with $N_{\rm sh} = 20$ major shells. The RQRPA configuration space was truncated using energy cutoffs of 180 MeV and 1800 MeV for the positive-energy two-quasiparticle configurations and the configurations involving negative-energy states, respectively. The same cutoff scheme was used for all isotopes and for the $J^\pi = 2^+, 3^-, 4^+$ multipolarities. The NLD energy bin width was set to 0.1 MeV. This numerical resolution captures the excitation-energy dependence of the combinatorial NLD while suppressing excessive bin-to-bin fluctuations associated with the discretized configuration spectrum. The maximum excitation energy was set to 10 MeV, covering the neutron separation-energy region and the range of the Oslo-normalized comparison used in this work.

The RQRPA is then constructed on the RHB vacuum to describe small-amplitude collective excitations. Its matrix equation is

$$\begin{pmatrix} A^J & B^J \\ -B^{*J} & -A^{*J} \end{pmatrix} \begin{pmatrix} X^{\nu,J} \\ Y^{\nu,J} \end{pmatrix} = \omega_\nu \begin{pmatrix} X^{\nu,J} \\ Y^{\nu,J} \end{pmatrix}, \tag{1}$$

where ω_ν is the excitation energy of the phonon state ν,

and $X^{\nu,J}$ and $Y^{\nu,J}$ are the forward- and backward-going two-quasiparticle amplitudes. The RQRPA calculations are performed for the multipolarities $J^\pi = 2^+$, 3^-, and 4^+. For each multipolarity, the RQRPA solutions are ordered by their excitation energies. The lowest positive-energy solution in each channel is identified as the first phonon state, denoted by 2^+_1, 3^-_1, and 4^+_1, respectively. Equivalently,

$$\omega_1^{J^\pi} = \min_\nu \left\{ \omega_{\nu,J^\pi} \mid \omega_{\nu,J^\pi} > 0 \right\}, \qquad J^\pi = 2^+, 3^-, 4^+. \quad (2)$$

The corresponding excitation energies are used directly as the microscopic phonon-energy inputs to the vibrational correction. The same energy-ordering criterion is applied to all selected Sn isotopes. No transition-strength criterion or adjustment of the experimental excitation energies is involved in the selection. Experimental excitation energies are used only for the external comparison in Table 1. The 4^+_1 input is used as the microscopic counterpart of the effective 4^+ channel in the adopted phenomenological vibrational prescription, and it should not be interpreted as evidence that this channel represents a purely hexadecapole one-phonon mode in every isotope.

Table 1. Phenomenological, RQRPA, and experimental excitation energies (MeV) of the low-lying 2^+_1, 3^-_1, and 4^+_1 states in selected even-even Sn isotopes. This comparison tests the physical energy scale of the empirical and microscopic phonon inputs; the experimental energies serve only as external references. The final two columns give the deviations from experiment, $\Delta_{\rm pheno} = E_{\rm pheno} - E_{\rm exp}$ and $\Delta_{\rm RQRPA} = E_{\rm RQRPA} - E_{\rm exp}$.

A	State	Phenom.	RQRPA	Exp.	$\Delta_{\rm pheno}$	$\Delta_{\rm RQRPA}$
	2^+_1	1.27	1.25	1.26	0.01	**−0.01**
112	3^-_1	1.95	2.26	2.35	−0.40	**−0.09**
	4^+_1	3.12	2.40	2.25	0.87	**0.15**
	2^+_1	1.18	1.41	1.29	−0.11	**0.12**
116	3^-_1	1.82	1.70	2.27	−0.45	**−0.57**
	4^+_1	2.92	2.67	2.39	0.53	**0.28**
	2^+_1	1.18	1.43	1.27	−0.09	**0.16**
118	3^-_1	1.82	1.80	2.32	−0.50	**−0.52**
	4^+_1	2.92	2.87	2.28	0.64	**0.59**
	2^+_1	1.22	1.47	1.17	0.05	**0.30**
120	3^-_1	1.87	2.02	2.40	−0.53	**−0.38**
	4^+_1	3.00	2.85	2.19	0.81	**0.66**
	2^+_1	1.29	1.50	1.14	0.15	**0.36**
122	3^-_1	1.99	2.32	2.49	−0.50	**−0.17**
	4^+_1	3.18	2.68	2.14	1.04	**0.54**
	2^+_1	1.42	1.52	1.13	0.29	**0.39**
124	3^-_1	2.19	2.67	2.10	0.09	**0.57**
	4^+_1	3.50	2.53	2.60	0.90	**−0.07**

B. Combinatorial NLD and vibrational correction

The RHB quasiparticle spectrum provides the microscopic input for the intrinsic combinatorial level density. For each single-particle level, the excitation energy ϵ, spin projection m, and parity p are used to enumerate particle–hole configurations under the Pauli principle. The resulting intrinsic state density $\rho_i(U, M, P)$ is obtained for a given excitation energy U, spin projection M, and parity P [35–38]. In this way, shell effects and level fluctuations enter the calculation directly through the microscopic single-particle spectrum.

The combinatorial formalism has been described in detail in Refs. [7, 18, 19, 22, 39, 40]. In the present work, we use the corresponding generating function

$$\mathcal{Z}(x_1, x_2, x_3, x_4, y, t) = \prod_{k=1}^{4} \prod_{i=1}^{I_k} \left(1 + x_k p_i^k y^{\varepsilon_i^k} t^{m_i^k}\right), \quad (3)$$

where y and t are associated with the excitation energy and spin projection, respectively, and x_k counts the proton and neutron particle and hole numbers. The quantities ε_i^k, m_i^k, and p_i^k denote the excitation energy, spin projection, and parity of the corresponding single-particle state.

Low-lying vibrational configurations are included using the generalized boson-partition-function prescription adopted in previous combinatorial NLD calculations [18, 19, 25, 39]. The corresponding boson partition function can be written as [19, 41]

$$\mathcal{Z}_{\rm boson} = \prod_{\lambda} \prod_{\mu=-\lambda}^{\lambda} \sum_{N_{\lambda\mu}=0}^{\infty} (y^{\epsilon_{\lambda\mu}} t^{\mu} p_\lambda)^{N_{\lambda\mu}}. \quad (4)$$

Here y, t, and p denote the phonon excitation energy, angular-momentum projection, and parity, respectively. The quantity $\epsilon_{\lambda\mu}$ is the energy of a phonon with multipolarity λ and projection μ, and p_λ is its parity. For the spherical phonon inputs considered here, $\epsilon_{\lambda\mu} = \omega_\lambda$. Thus, the phonon excitation energy enters explicitly into the boson partition function and determines the excitation-energy values at which the corresponding vibrational configurations become accessible.

Expanding the boson partition function generates vibrational configurations resolved in excitation energy, angular-momentum projection, and parity. Their state density is folded with the intrinsic particle–hole state density to obtain the intrinsic-vibrational state density $\rho_{i*\nu}(U, M, P)$, following the established prescription of the

cited works. In the present numerical implementation, the phonon expansion is truncated at the four-phonon level. This truncation is sufficient for the excitation-energy range up to 10 MeV considered in the present work, whereas calculations extending to higher excitation energies require the inclusion of higher-order phonon configurations. No additional microscopic phonon–quasiparticle interaction is introduced in the present calculation.

For the spherical nuclei considered here, the final spin-parity-resolved level density is obtained from the projection-resolved state density as [25]

$$\rho(U,J,P) = \rho_{i*\nu}(U,M=J,P) - \rho_{i*\nu}(U,M=J+1,P). \quad (5)$$

The phonon excitation energies enter the boson partition function and thereby determine the excitation-energy locations of the generated vibrational configurations. The same partition function, intrinsic-vibrational folding, and subsequent state counting are used in the phenomenological and RQRPA-based calculations.

The phenomenological vibrational correction used as a reference follows Refs. [18, 39]. This prescription represents precisely the empirical component that is replaced by the RQRPA phonon energies in the microscopic calculation. In this prescription, the collective phonon energies are not obtained from a microscopic response calculation but are estimated from empirical mass-dependent systematics. The leading mass dependence is written as

$$\omega_\lambda \propto A^{-5/6}, \quad (6)$$

with coefficients chosen to reproduce the typical energies of low-lying collective states.

For the 2^+, 3^-, and 4^+ vibrational modes, the corresponding energies are

$$\omega_2 = \frac{65A^{-5/6}}{1+0.05E_{\rm shell}}\ {\rm MeV}, \quad (7)$$

$$\omega_3 = \frac{100A^{-5/6}}{1+0.05E_{\rm shell}}\ {\rm MeV}, \quad (8)$$

$$\omega_4 = \frac{160A^{-5/6}}{1+0.05E_{\rm shell}}\ {\rm MeV}. \quad (9)$$

Here, the shell-correction energy is defined as

$$E_{\rm shell} = E_{\rm tot} - E_{\rm LD}, \quad (10)$$

where $E_{\rm tot}$ and $E_{\rm LD}$ denote the microscopic total energy and the liquid-drop reference energy, respectively. These expressions define the empirical phonon-energy scale of the reference calculation.

The controlled replacement is therefore

$$\omega_\lambda^{\rm pheno} \longrightarrow \omega_{1,\lambda}^{\rm RQRPA}, \qquad \lambda = 2,3,4. \quad (11)$$

The intrinsic combinatorial spectrum, the boson-partition prescription, the numerical truncations, and the subsequent state counting are identical in the two calculations. Therefore, any difference between the phenomenological and RQRPA-based NLDs arises solely from the replacement of the phonon-energy inputs.

III. RESULTS AND DISCUSSION

We present the results as a controlled test of the microscopic replacement. First, we compare the empirical and RQRPA phonon-energy scales. We then show how the adopted microscopic phonons modify the NLD in a representative isotope. The full RQRPA-based NLDs are subsequently benchmarked against the phenomenological prescription and Oslo-normalized data. Finally, a channel diagnostic near the neutron separation energy is used to identify how the 2^+, 3^-, and effective 4^+ inputs contribute to the effective enhancement. In all comparisons, the intrinsic combinatorial density and the combinatorial vibrational prescription are kept fixed.

A. Empirical and microscopic phonon-energy scales

The first step is to verify that the microscopic phonons provide a physically comparable energy scale to the empirical inputs they replace. This comparison is a scale-consistency check rather than a fit: the experimental levels are used only to assess whether the empirical and RQRPA inputs lie within the observed low-lying collective-energy window. Table 1 lists the phenomenological, RQRPA, and experimental energies of the low-lying 2_1^+, 3_1^-, and 4_1^+ states. The experimental values are taken from NuDat 3.0 [28] and are used only as references for known nuclei; they are not included in the vibrational correction or used to tune the RQRPA phonon energies.

The table indicates that both prescriptions place the relevant phonon energies on the MeV scale of the observed low-lying collective states. This agreement in scale is the relevant condition for the replacement test, because the NLD calculation uses these energies as collective inputs rather than as fitted observables. However, the isotope- and multipolarity-dependent deviations differ. The phenomenological prescription follows a smooth mass-dependent trend, whereas the RQRPA energies reflect the nucleus-dependent microscopic response of the RHB ground state. This is the essential difference between the two inputs: the empirical scale is replaced by

a self-consistent response calculation, without changing the intrinsic combinatorial density.

Before turning to the systematic benchmark, we illustrate how the microscopic phonon input enters the NLD. Figure 1 presents ^{118}Sn as a representative case. The adopted RQRPA 2^+_1, 3^-_1, and 4^+_1 modes are included separately on top of the same intrinsic combinatorial density, while the full RQRPA result includes all three modes.

The low-lying 2^+_1 and 3^-_1 modes provide comparable single-mode enhancements in ^{118}Sn, whereas the 4^+_1 mode yields a smaller contribution. This indicates that the relative importance of vibrational channels is not determined solely by multipolarity. Rather, the enhancement depends on the combined effects of the phonon excitation energy, the spin-parity structure in the combinatorial state counting, and the underlying intrinsic quasiparticle level-density distribution. The 2^+ channel often provides a large effective contribution in the isotopic systematics, but it does not dominate in every individual isotope.

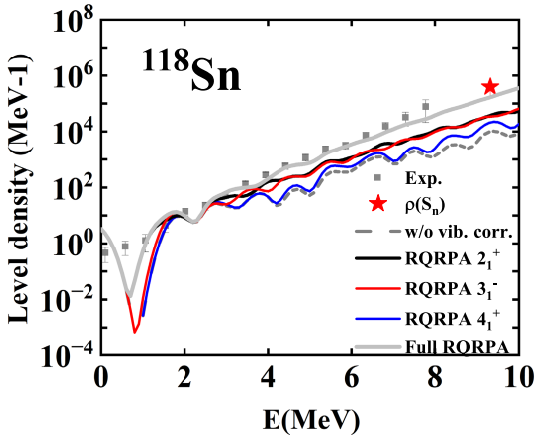


Fig. 1. (color online) Representative single-mode response of the NLD to the RQRPA phonon input in ^{118}Sn. The grey dashed line denotes the intrinsic combinatorial density without vibrational enhancement. Solid curves show calculations in which the adopted RQRPA modes are included separately, while the full RQRPA result includes all three modes. Red pentagrams denote the adopted $\rho(S_n)$ constraint.

The phonon correction also produces a smoothing effect on the intrinsic combinatorial NLD. The intrinsic density contains local fluctuations associated with the discrete quasiparticle-configuration spectrum. Folding these intrinsic configurations with low-lying vibrational states introduces additional shifted configurations, and the superposition of these contributions reduces local fluctuations, thereby producing smoother NLD curves.

B. Preservation of the phenomenological enhancement

The decisive test is whether replacing the empirical phonon energies with RQRPA phonons approximately preserves the NLD systematics obtained using the phenomenological vibrational correction. Figure 2 compares the intrinsic combinatorial density, the phenomenologically corrected NLD, and the RQRPA-based NLD with the Oslo-normalized data for the selected even-even Sn isotopes. The adopted $\rho(S_n)$ constraints follow the Oslo normalization in Ref. [29]. The isotope ^{114}Sn is not included because the corresponding Oslo-normalized level-density data are not available.

The RQRPA-based correction provides a description comparable to that of the phenomenological prescription

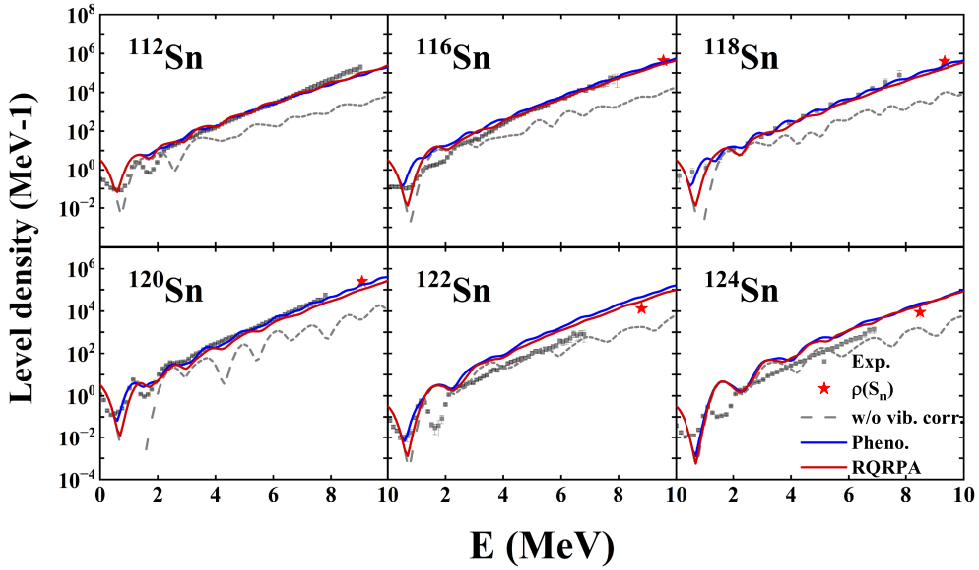


Fig. 2. (color online) Benchmark of the microscopic replacement in selected even-even Sn isotopes. The Oslo-normalized level densities are compared with the intrinsic combinatorial density without vibrational correction, the phenomenological vibrational prescription, and the RQRPA-based replacement of the empirical phonon inputs. Red stars denote the adopted $\rho(S_n)$ constraints.

for most of the selected isotopes. This agreement is the central benchmark of the present work. It shows that the average vibrational enhancement encoded in the empirical phonon-energy systematics can be approximately recovered when the empirical phonon energies are replaced by microscopic RQRPA values. The calculation tests whether the phonon-energy input can be made microscopic without changing the successful average behavior of the phenomenological prescription.

The isotope-dependent differences between the phenomenological and RQRPA-based calculations originate from the different phonon excitation energies listed in Table 1. A lower RQRPA phonon energy enhances the accessibility of the corresponding phonon-folded configurations, whereas a higher phonon energy reduces this contribution. Although the individual phonon-channel contributions can differ significantly, the total NLD includes contributions from several collective modes. Therefore, partial compensation among different channels leads to relatively small differences between the final phenomenological and RQRPA-based NLD curves, while larger differences remain visible in the channel-resolved analysis. Thus, Fig. 2 tests the stability of the total vibrational enhancement, whereas Fig. 3 shows how that enhancement is redistributed among the adopted collective channels.

For the heavier isotopes, especially ^{122,124}Sn, both corrected calculations tend to overestimate the Oslo-normalized level densities. Since this behavior appears in both the phenomenological and RQRPA-based results, it is unlikely to originate solely from the microscopic replacement of the phonon energies. It may instead reflect limitations of the intrinsic single-particle spectrum, pairing correlations, spin-parity distribution, or the absence of excitation-energy-dependent damping of the vibrational enhancement. This point does not alter the replacement test, but it indicates where further improvements of the underlying NLD model are needed.

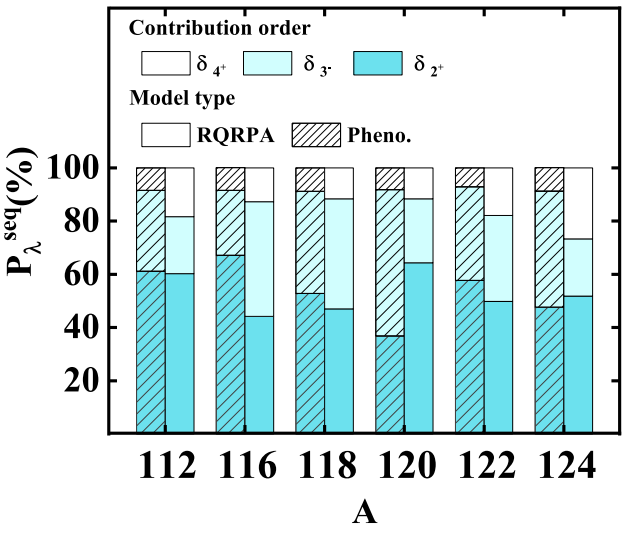


Fig. 3. (color online) Sequential channel diagnostics of the logarithmic enhancement of $\rho(S_n)$. The stacked components δ_2, δ_3, and δ_4 denote the 2^+, 3^-, and effective 4^+ channels, respectively. For the phenomenological calculation, the channel energies are taken from empirical 2^+, 3^-, and 4^+ systematics, whereas in the microscopic replacement they are taken from the RQRPA 2^+_1, 3^-_1, and 4^+_1 phonon energies. The percentages are obtained with the fixed inclusion order $2\to3\to4$ and should be interpreted as effective, order-dependent diagnostics rather than order-independent phonon strengths.

The similarity of the total NLDs motivates a channel-level diagnostic of how the empirical and microscopic phonon inputs construct the final enhancement.

C. Channel diagnostics near the neutron separation energy

The similarity of the total NLDs does not imply identical channel compositions. Because the phenomenological and RQRPA-based calculations employ different phonon energies, the effective contribution of each vibrational channel may differ even when the final NLDs are similar. We therefore use a sequential logarithmic decomposition of $\rho(S_n)$ as a diagnostic of the adopted vibrational prescription.

The contribution hierarchy is not determined solely by phonon excitation energy or multipolarity. A lower phonon excitation energy reduces the energetic cost of generating phonon-folded configurations and generally increases their accessibility. The phonon angular momentum and parity determine how these configurations populate the spin-parity-resolved intrinsic level-density space, whereas the underlying quasiparticle distribution determines the available phase space. For the selected Sn isotopes, the relatively low 2^+ excitation energies, together with the corresponding spin-parity coupling and intrinsic phase space, often lead to a relatively large effective 2^+ increment in the adopted sequential diagnostic.

This decomposition is not intended to define unique, order-independent phonon strengths. Rather, it measures the logarithmic enhancement accumulated when the 2^+, 3^-, and effective 4^+ channels are added in the fixed order $2\to3\to4$. The superscripts (0), (2), (2+3), and (2+3+4) denote calculations without vibrational correction, with only the 2^+ channel, with the 2^+ and 3^- channels, and with all three collective channels included, respectively:

$$\delta_2 = \ln\frac{\rho^{(2)}(S_n)}{\rho^{(0)}(S_n)}, \tag{12}$$

$$\delta_3 = \ln\frac{\rho^{(2+3)}(S_n)}{\rho^{(2)}(S_n)}, \tag{13}$$

$$\delta_4 = \ln \frac{\rho^{(2+3+4)}(S_n)}{\rho^{(2+3)}(S_n)}. \tag{14}$$

The corresponding sequential effective percentage is defined as

$$P_\lambda^{\rm seq} = \frac{\delta_\lambda}{\delta_2+\delta_3+\delta_4} \times 100\%, \qquad \lambda = 2,3,4. \tag{15}$$

Here $\lambda = 2,3,4$ labels the 2^+, 3^-, and effective 4^+ channels. In the phenomenological calculation, the channel energies are taken from the empirical 2^+, 3^-, and 4^+ systematics. In the microscopic calculation, they are replaced by the RQRPA 2_1^+, 3_1^-, and 4_1^+ phonon energies. Figure 3 presents the resulting sequential diagnostic.

Within the adopted sequential diagnostic, the 2^+ channel provides the leading effective increment in most cases, while the 3^- and effective 4^+ channels provide additional corrections. The relative percentages differ between the phenomenological and RQRPA-based calculations because the phonon-energy scales are not identical. These differences provide a channel-level view of the microscopic replacement, but they should be interpreted only as diagnostics of the present prescription, rather than as unique phonon strengths.

IV. CONCLUSIONS AND OUTLOOK

We performed a controlled microscopic replacement of the empirical phonon-energy inputs used in combinatorial nuclear level-density calculations. The intrinsic RHB-based combinatorial density and the combinatorial vibrational prescription were kept fixed, while the phenomenological 2^+, 3^-, and 4^+ phonon energies were replaced with RQRPA-calculated 2_1^+, 3_1^-, and 4_1^+ phonon energies in selected even-even Sn isotopes.

The main result is that this replacement approximately preserves the average vibrational enhancement of the phenomenological prescription in the selected semi-magic Sn isotopes. The RQRPA-based NLDs remain close to the phenomenologically corrected NLDs and provide a comparable description of the Oslo-normalized constraints. This finding indicates that the average enhancement encoded in the phenomenological prescription is broadly compatible with the low-lying collective response obtained microscopically within the same RHB-based framework.

Within the adopted sequential diagnostic, the 2^+ channel often provides the leading effective increment, while the 3^- and effective 4^+ channels provide additional corrections. The extracted channel percentages depend on the fixed inclusion order and should therefore be viewed as diagnostics of the adopted vibrational prescription, rather than as order-independent phonon strengths.

The present work provides a practical route for constructing microscopic phonon-energy inputs for vibrationally corrected combinatorial NLD calculations. The present benchmark indicates that experimental low-lying phonon energies need not be used as direct collective inputs for the vibrational correction in the selected Sn isotopes. This feature is important for applying combinatorial NLD models to nuclei for which spectroscopic information is incomplete. Future work should address excitation-energy-dependent damping of collective enhancement, extensions to deformed nuclei with a separate treatment of rotational collectivity, and the propagation of the resulting microscopic NLDs into reaction observables.

ACKNOWLEDGMENTS

The authors are grateful to Yangping Shen (China Institute of Atomic Energy) for his support in the reliability analysis of the experimental data, Dongfeng Chen (China Institute of Atomic Energy) for valuable discussions and technical support. They also thank Pengxiang Du (Jilin University) for helpful guidance and constructive discussions, and Xiaofei Jiang (Peking University) for useful advice.

References

[1] H. A. Bethe and R. F. Bacher, Rev. Mod. Phys. **8**, 82 (1936)
[2] H. A. Bethe, Rev. Mod. Phys. **9**, 69 (1937)
[3] E. Beták and J. Dobeš, Zeitschrift für Physik A **279**, 319 (1976)
[4] F. C. Williams, Nucl. Phys. A **166**, 231 (1971)
[5] P. Obložinský, Nucl. Phys. A **453**, 127 (1986)
[6] W. Dilg, W. Schantl, H. Vonach, and M. Uhl, Nucl. Phys. A **217**, 269 (1973)
[7] A. Koning, S. Hilaire, and S. Goriely, Nucl. Phys. A **810**, 13 (2008)
[8] A. V. Ignatyuk, Tech. Rep. INDC(CCP)-233/L, IAEA (1985).
[9] A. V. Ignatyuk, Tech. Rep. TECDOC-1034, IAEA (1998).
[10] S. Goriely, Nucl. Phys. A **605**, 28 (1996)
[11] Y. Alhassid, S. Liu, and H. Nakada, Phys. Rev. Lett. **83**, 4265 (1999)
[12] W. E. Ormand, Phys. Rev. C **56**, R1678 (1997)
[13] J. A. White, S. E. Koonin, and D. J. Dean, Phys. Rev. C **61**, 034303 (2000)
[14] N. Cerf, Phys. Rev. C **49**, 852 (1994)
[15] N. Cerf, Phys. Rev. C **50**, 836 (1994)
[16] B. K. Agrawal and A. Ansari, Nucl. Phys. A **640**, 362 (1998)
[17] S. Hilaire, S. Goriely, and S. Péru, EPJ Web of Conferences **322**, 06001 (2025)
[18] S. Hilaire and S. Goriely, Nucl. Phys. A **779**, 63 (2006)
[19] S. Goriely, S. Hilaire, and A. J. Koning, Phys. Rev. C **78**, 064307 (2008)

[20] S. Goriely, S. Hilaire, and A. J. Koning, Astronomy & Astrophysics **487**, 767 (2008)
[21] S. Goriely, A.-C. Larsen, and D. Mücher, Phys. Rev. C **106**, 044315 (2022)
[22] S. Hilaire, M. Girod, S. Goriely *et al.*, Phys. Rev. C **86**, 064317 (2012)
[23] K.-P. Geng, P.-X. Du, J. Li *et al.*, Nucl. Sci. Tech. **34**, 141 (2023)
[24] X. Jiang, X. Wu, P. Zhao *et al.*, Phys. Lett. B **849**, 138448 (2024)
[25] G. He, N. Tang, Y. Tian *et al.*, Chin. Phys. C **50**, 054107 (2026)
[26] D. Vretenar, A. V. Afanasjev, G. A. Lalazissis *et al.*, Physics Reports **409**, 101 (2005)
[27] N. Paar, P. Ring, T. Nikšić *et al.*, Phys. Rev. C **67**, 034312 (2003)
[28] National Nuclear Data Center, Nudat 3.0, https://www.nndc.bnl.gov/nudat3/, accessed: July 2, 2026.
[29] M. Markova, A. C. Larsen, P. von Neumann-Cosel *et al.*, Phys. Rev. C **109**, 054311 (2024)
[30] B. D. Serot, Reports on Progress in Physics **55**, 1855 (1992)
[31] P.-G. Reinhard, Reports on Progress in Physics **52**, 439 (1989)
[32] B. D. Serot and J. D. Walecka, in *Advances in Nucl. Phys. Vol. 16*, edited by J. W. Negele and E. Vogt (New York: Plenum Press, 1986), p. 1
[33] Y. Tian, Z. Ma, and P. Ring, Phys. Lett. B **676**, 44 (2009)
[34] Y. Tian, Z. Y. Ma, and P. Ring, Phys. Rev. C **79**, 064301 (2009)
[35] B. Strohmaier, S. M. Grimes, and H. Satyanarayana, Phys. Rev. C **36**, 1604 (1987)
[36] S. M. Grimes and T. N. Massey, Phys. Rev. C **51**, 606 (1995)
[37] J. B. French and K. F. Ratcliff, Phys. Rev. C **3**, 94 (1971)
[38] P. Decowski, W. Grochulski, A. Marcinkowski *et al.*, Nucl. Phys. A **110**, 129 (1968)
[39] S. Hilaire, J. P. Delaroche, and M. Girod, The European Physical Journal A **12**, 169 (2001)
[40] S. Goriely, M. Samyn, and J. M. Pearson, Phys. Rev. C **75**, 064312 (2007)
[41] S. Hilaire, S. Goriely, S. Péru *et al.*, Phys. Lett. B **843**, 137989 (2023)